



HAL
open science

Silicon coating on very dense tungsten particles by fluidized bed CVD for nuclear application

Florence Vanni, Brigitte Caussat, Carine Ablitzer, Xavière Iltis, Méryl Bothier

► To cite this version:

Florence Vanni, Brigitte Caussat, Carine Ablitzer, Xavière Iltis, Méryl Bothier. Silicon coating on very dense tungsten particles by fluidized bed CVD for nuclear application. *physica status solidi (a)*, 2015, 212 (7), pp.1599-1606. 10.1002/pssa.201532304 . cea-02385799

HAL Id: cea-02385799

<https://cea.hal.science/cea-02385799>

Submitted on 23 Nov 2023

HAL is a multi-disciplinary open access archive for the deposit and dissemination of scientific research documents, whether they are published or not. The documents may come from teaching and research institutions in France or abroad, or from public or private research centers.

L'archive ouverte pluridisciplinaire **HAL**, est destinée au dépôt et à la diffusion de documents scientifiques de niveau recherche, publiés ou non, émanant des établissements d'enseignement et de recherche français ou étrangers, des laboratoires publics ou privés.

Silicon coating on very dense tungsten particles by fluidized bed CVD for nuclear application

Florence Vanni^{1,2}, Brigitte Caussat^{*,2}, Carine Ablitzer^{**,1}, Xavière Iltis¹, and Méryl Bothier¹

¹ CEA Cadarache, DEN/DEC, Laboratoire des Combustibles Uranium, 13108 Saint-Paul-Lez-Durance, France

² University of Toulouse, Laboratoire de Génie Chimique, UMR CNRS 5503, ENSIACET/INPT, 4 allée E. Monso, BP 44362, 31432 Toulouse Cedex 4, France

Keywords CVD, fluidized bed, silane, silicon

* Corresponding author: e-mail brigitte.caussat@ensiacet.fr, Phone: +33 534 323 632, Fax: +33 534 323 697

** e-mail carine.ablitzer@cea.fr, Phone: +33 442 257 463, Fax: +33 442 254135

Tungsten particles were coated by silicon from silane (SiH_4) at 645 °C using fluidized bed chemical vapor deposition (FB-CVD). The coated particles were made from a surrogate tungsten powder and showed a median diameter (75 μm) and density (19,300 kg/m^3). We studied the behavior of these tungsten particles due to their similarity with U(Mo) particles which are being investigated for use as fuel in research reactors. The results show that the fluidized bed's thermal gradient and pressure drop both increase as soon as silane is injected into the reactor. These phenomena are linked to the reactivity of silane and the very high density of the tungsten powder, and they represent a risk of bed

agglomeration. A low inlet molar fraction of silane (0.5%) makes it possible to limit this risk. An increase in the fluidizing gas velocity and a decrease in the reactor diameter from 3.8 to 3.0 cm, have little impact on these phenomena for the operating range studied. Characterizations (EDX, SEM, XRD, etc.) show that all the tungsten particles are uniformly coated by a continuous film of silicon, mainly crystallized and of nodular morphology. The thickness of this silicon layers varies between 0.1 and 1 μm , which corresponds to the target. As the feasibility of the coating has been demonstrated, new experiments are in progress with fissile particles.

1 Introduction This study concerns the coating of tungsten particles by a silicon layer, using the fluidized bed CVD process. Tungsten particles were chosen for this study as a surrogate powder for economic and safety reasons, because they present characteristics close to those of the U(Mo) powder, a metallic nuclear fuel, currently being studied as part of the development of research reactors. In the nuclear field, the development of material testing reactors (MTR) has led to studies on fuel plates containing a pulverulent metal fuel made of U(Mo) particles.¹ The concept currently selected is based on the dispersion of U(Mo) particles in an aluminum matrix, which is then covered with two aluminum sheets to form the fuel plates. Since the late 90s, irradiation campaigns have been carried out in France, Belgium, the United States, South Korea,

Canada, and Russia, to qualify the behavior of the plates under irradiation. The results of some of these programs, such as RERTR [1, 2], IRIS [3, 4], KOMO [5], E-FUTURE [6, 7], and SELENIUM [8, 9] irradiations, show that adding a silicon deposit on the surface of the U(Mo) particles would improve the behavior of the fuel plates under irradiation, at high burn-up. The unstable behavior of U(Mo) fuel under irradiation is associated with the development of an amorphous interaction layer between the U(Mo) particles and the Al matrix. This layer is unable to retain the fission gases created. Gas bubbles migrate to the interface between the interaction layer and the matrix where they percolate, thus causing swelling or even destruction of the fuel element. A silicon layer on U(Mo) particles would reduce these interaction phenomena by a barrier effect. The targeted thickness of this layer ranges between 100 nm and 1 μm , as defined on the basis of previous irradiation programs [1–9].

¹ U(Mo): uranium–molybdenum binary alloy with ~8 wt% of molybdenum.

1.1 Choice of the coating process To choose the process for depositing the Si layer on the U(Mo) powder, it was necessary to consider several criteria. Firstly, the process had to be compatible with the physico-chemical properties of the U(Mo) material. Secondly, this process had to produce to a silicon layer of adequate adhesion, quality, and thickness.

Two processes were identified: physical vapor deposition (PVD) and chemical vapor deposition (CVD). PVD silicon-coated U(Mo) particles underwent irradiation tests in 2010 and produced some promising results (see the SELENIUM irradiation program [10]). Fluidized bed chemical vapor deposition (FB-CVD) is another process that can be used to coat U(Mo) particles with Si, which is what we chose to investigate in our study. By energetically mixing the particles in the bed, the fluidized bed optimizes contact between the gas phase and the divided solid, favoring mass and heat transfers [11], while allowing the uniform deposition of the material on the powders at high deposition rates [12].

1.2 Precursor FB-CVD allows for a large choice of precursors in the case of silicon deposits. The main precursors are organosilanes [13, 14] which are mainly used for SiC deposits, chlorosilanes [15, 16] for corrosion-resistant materials, and silanes [17, 18]. These last precursors include silane (SiH_4), disilane (Si_2H_6), and trisilane (Si_3H_8). The coating time can be reduced when disilane or trisilane is used instead of silane. However, these precursors are more expensive and result in the formation of a larger amount of fines.

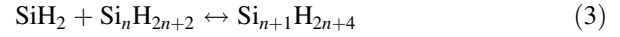
Silane pyrolysis includes two types of chemical reactions in proportions that depend on the deposition conditions. The first type involves homogeneous reactions: Onischuk et al. [19] explain that silane, via gaseous by-products, leads to the nucleation of hydrogenated silicon nanoparticles, named fines. Some of these fines can be scavenged by the bed particles to contribute to deposition. The remainder is lost; it is either stuck on the reactor walls or removed by elutriation. This remainder reduces the amount of silicon deposited in the bed and therefore the global conversion rate of the process. Though the formation mechanism of fines is not yet fully elucidated, authors like Swihart et al. [20] and Talukdar et al. [21] have quantified the nucleation process in gas phase, the growth and aggregation of fines with a model based on the successive addition of saturated or unsaturated polysilanes, forming cyclic polysilanes resulting in hydrogenated silicon clusters.

The second type of reactions concerns heterogeneous reactions which take place directly on the surface of the particles [22].

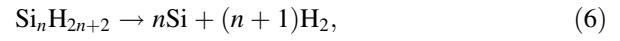
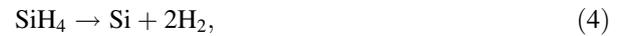
Most authors like Hogness et al. [23] agree that silane pyrolysis occurs from 370 °C. The first homogeneous decomposition step involves the following reactions



Differences of opinion exist between the authors [24–26], but reaction (1) is mainly considered as the initiator of numerous homogeneous chain reactions which can produce fines. Silylene (SiH_2) is a highly reactive radical species which reacts with silane to form polysilanes



According to Cadoret et al. [27], silylene (SiH_2) in a fluidized bed with good gas solid contact should be preferably consumed in the heterogeneous phase due to the high specific surface area of the substrates, rather than in the homogeneous phase. Filtvedt et al. [28] claim that the formation of fines is highly dependent on the silane concentration. Silane and its by-products decompose heterogeneously according to the following reactions



These reactions contribute to the deposit with different kinetics and in proportions depending on the experimental conditions, including the temperature, the inlet molar fraction of silane, and the specific surface area of the substrates.

1.3 Characteristics of the powder and aim of the study FB-CVD experiments were performed on a surrogate powder: a tungsten powder with a density of 19,300 kg/m³ – similar to that of U(Mo) (17,500 kg/m³) – and a mean grain diameter of 75 μm compared with 50 μm for U(Mo).

The tungsten powder is very dense, which explains its non-optimal fluidization. This results in the small expansion of the fluidized bed and low particle mobility compared with Geldart's easy-to-fluidize group A or B powders [29], mainly used in the field of fluidization. This is why it was necessary to analyze the feasibility of coating extremely dense powders by silicon FB-CVD. This involved studying the influence of the key parameters on the process behavior and on the coating characteristics. Another constraint was to use powder weights as low as possible for safety and economic reasons. This paper discusses the impact of the reactor diameter, the inlet molar fraction of silane, and the fluidizing gas velocity.

2 Experimental We tested two CVD reactors (Fig. 1) which comprised vertical steel tubes with inner diameters of 3.8 and 3.0 cm and were 1 m in height. The reactors were heated by an external furnace and the temperature was controlled by two thermocouples fixed on the outer wall of the reactors. The fluidization gas was argon (Air Liquide, Alpha 1), controlled by an Aera FC-7710 CO mass flowmeter. The ascendant stream of argon went through a porous steel distributor to fluidize the tungsten particles. During deposition, silane (Air Liquide, N50) was added to argon and controlled by a Brooks rota-meter.

Five thermocouples were placed in the reactor inside a steel tube with an inner diameter of 6 mm. They measured the temperature at different heights in the fluidized bed with an uncertainty of $\pm 2.5^\circ\text{C}$, and were located at 1, 2.5, 5, 7, and 12 cm above the distributor respectively. A sixth thermocouple was placed under the distributor. A LPX 5380 GE Druck sensor measured the bed pressure drop (at $\pm 1.8\%$) with taps under the distributor and at the top of the reactor. All measurements were registered in real time by the DasyLab[®] acquisition system.

2.1 Powder used The tungsten powder used was provided by NEYCO (CERAC, Inc., T-1220). Observations by scanning electron microscopy (FEI Nova Nano SEM 450) revealed that the particles were faceted and not spherical (Fig. 2). Laser grain size measurements in dry mode (Malvern MasterSizer Sirocco 2000) indicated that the distribution of the particle diameters d_{10}/d_{90} was 40/105 μm with a median diameter of 75 μm .

2.2 Operating conditions The operating conditions are described in Table 1. The average target temperature in the fluidized bed was 645°C for all experiments. The decrease in the reactor diameter from 3.8 to 3.0 cm was studied to reduce the mass of powder treated for economic and safety reasons.

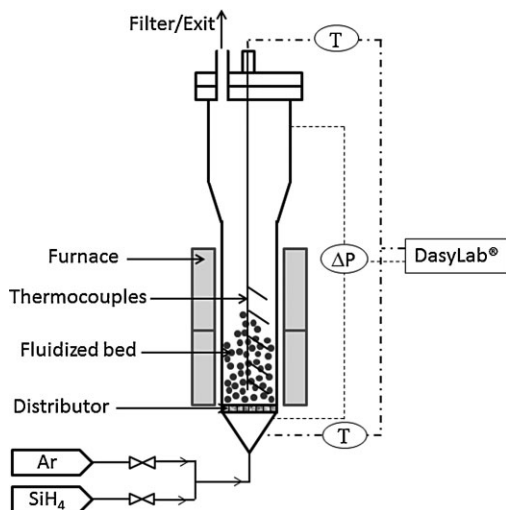


Figure 1 Schematic diagram of the FB-CVD reactor.

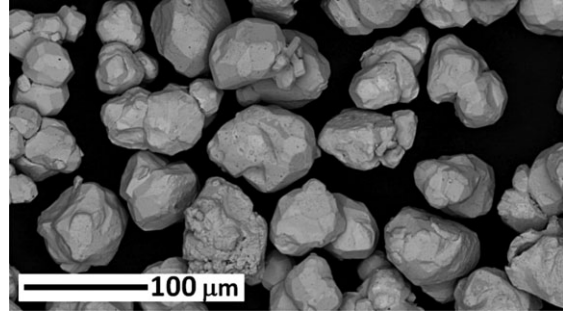


Figure 2 SEM view of the tungsten particles.

The ratio between the fixed bed height and the reactor diameter H_0/D was fixed at three since this ratio allows for optimal heat transfers in the bed according to Rodriguez et al. [30]. This led to powder weights of 1500 and 740 g for reactor diameters of 3.8 and 3.0 cm, respectively.

The minimum fluidization velocity U_{mf} was 3 cm/s, which was determined by studying the fluidization of the tungsten powder at room temperature [30]. A fluidization ratio U_g/U_{mf} close to or higher than five ensures appropriate gas-powder contact for CVD on these powders [30].

The inlet molar fraction of silane was varied from 0.5 to 5.2%. The deposit duration, ranging from 60 to 180 min, was chosen to obtain silicon thicknesses between 100 nm and 1 μm , with this range corresponding to the target for the final application.

2.3 Sample preparation techniques In order to analyze the composition and the thickness of the Si deposit, scanning electron microscopy (SEM), energy-dispersive X-ray spectroscopy (EDX), X-ray diffraction (XRD), and transmission electron microscopy/scanning transmission electron microscopy examinations (TEM-STEM) were performed on samples.

Two sample preparation methods were used for examining the coating by SEM. The first method consisted in crushing the coated tungsten powder in order to partially detach the Si layer from its substrate. Areas of damaged particles where the Si layer was visible in the cross section

Table 1 Operating conditions.

run	reactor diameter \emptyset	mass of powder m_0	fluidization ratio	inlet molar fraction of SiH_4 y_{silane}
	[cm]	[g]	$[U_g/U_{mf}]$	[%]
1	3.8	1500	4.7	0.5
2	3.8	1500	4.7	2.6
3	3.8	1500	4.7	4.0
4	3.8	1500	4.7	5.2
5	3.8	1500	6	0.5
6	3.0	740	4.7	0.5
7	3.0	740	6	0.5

were then examined. The second method consisted in embedding the coated powder in an aluminum matrix and mechanically polishing the composite to obtain cross views of the coated area. This technique is more time-consuming, but its results are more precise.

TEM-STEM analyses were performed on thin sections that were 20 μm wide and 5 μm deep, prepared from particles coated using the focused ion beam (FIB) method.

3 Results and discussion

3.1 Changes in the thermal gradient and pressure drop with the inlet molar fraction of silane As soon as silane was injected into the reactor, a thermal gradient between the bottom and the top of the fluidized bed often appeared during our experiments. The term “thermal gradient” describes the temperature difference registered by the thermocouples placed at 1 and 7 cm above the distributor in the fluidized bed.

Figure 3 shows the changes in the thermal gradient during runs 1–4, for various inlet molar fractions of silane in the 3.8 cm reactor.

Whereas it did not exceed 15 $^{\circ}\text{C}$ before silane injection, a gradient peak of 25–50 $^{\circ}\text{C}$ rapidly appeared after silane injection for inlet molar fractions of at least 2.6%. This peak decreased after a few minutes and then the thermal gradient regularly decreased throughout the deposition process. No thermal gradient appeared with a molar fraction of 0.5%.

It is well-known that silicon CVD from silane has a reversible impact on the bed thermal profile and pressure drop due to the partial de-fluidization of the bed, which is probably related to the appearance of short-lived agglomerates. Silicon dangling bonds can form on the surface of each particle during deposition, acting as glue for the surrounding particles [31, 32]. This creates ephemeral agglomerates that can disrupt particle mixing and therefore affect heat transfers in the fluidized bed [28]. Similar observations were made by Ruvalcaba et al. [33] and Tejero-Ezpelata et al. [34] for low fluidizing gas velocities and for inlet molar fractions of silane higher than 7%. This phenomenon is therefore clearly more marked for the tungsten powder, which is probably due to its very high density. The low particle mobility can promote the ephemeral agglomeration previously mentioned, compared with conventional Geldart’s A or B particles usually treated by this process, since their density is generally six times lower (for similar median diameters) than the density of tungsten powder.

In addition to this thermal gradient phenomenon, a bed pressure drop peak appeared as soon as silane was injected into the reactor.

Before silane injection, the bed pressure drop remained similar to the theoretical bed pressure drop corresponding to the weight of powder per column surface area, i.e., around 140 mbar. After injection, a ΔP peak appeared proportional to the molar fraction of silane, reaching 10–50 mbar. This peak always appeared concomitantly with the thermal gradient peak. The pressure drop then regularly decreased

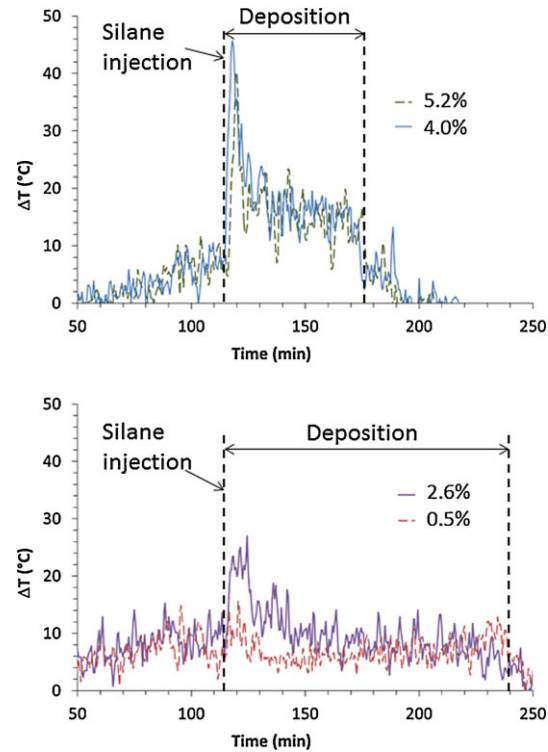


Figure 3 Changes in the thermal gradient for various inlet molar fractions of silane (\varnothing 3.8 cm, $U_g/U_{mf} = 4.7$, 645 $^{\circ}\text{C}$).

throughout the deposition process, as did the thermal gradient. This observation confirms the assumption of ephemeral agglomerates formation during deposits, which is proportional to the silane concentration.

Different inter-particles forces can co-exist in a fluidized bed, which are either repulsive like the solid collision forces, or attractive like the Van der Waals or the electrostatic forces. In the case of silicon deposition from silane, a specific attractive force seems to appear, related to the deposition chemistry on the particle surface. As long as the repulsive forces are higher than the attractive ones, at worse only partial de-fluidization is observed, leading to higher bed pressure drops and thermal gradients. The number of Si dangling bonds per unit surface area of powder is likely to increase with the silane concentration, leading to more marked bed disturbances. For an inlet molar fraction of silane of 0.5%, the number of Si dangling bonds is probably so low that bed disturbances are weak.

3.2 Effect of the reactor diameter and the fluidizing gas velocity An increase in the fluidizing gas velocity makes it possible to better mix particles before exalting heat and mass transfers, but it also involves a shorter gas residence time in the reactor.

When comparing runs 1 and 5 with runs 6 and 7, it can be seen that the fluidizing gas velocity was increased from 4.7 to 6 U_{mf} for an inlet silane molar fraction of 0.5%, in the

3.8 and 3.0 cm diameter reactors respectively. Figure 4 shows the changes in the bed thermal gradient for these runs.

By increasing the fluidizing gas velocity, the thermal gradient can be reduced by 2–3 °C during the deposit, but it has negligible impact on the pressure drop. This means that the gas–solid contact is improved slightly by the gas velocity increase, but the balance between the inter-particle attractive forces (due to Si deposition) and the repulsive forces existing in the bed is not significantly modified by this increased flow rate.

However, a reduced reactor diameter enhances the thermal gradient by about 10 °C during deposits, which means that there is a more marked risk of agglomeration in the 3 cm diameter reactor. This can be explained by the fact that wall effects are greater in this small reactor, with particle/wall friction phenomena which decrease the gas-powder contact in the bed. The pressure drop remained stable during these runs because the inlet molar fraction of silane was very low (0.5%).

3.3 State of the powder after runs Laser grain size analyses were performed after each run, showing that there was no agglomeration of tungsten particles.

Figure 5 shows the bed of particles just after emptying the reactor following runs 1–4. The initial tungsten powder was black but became a blue gray color after Si coating. For runs with inlet molar fractions of silane higher than 0.5%, brown residues were found in the reactor. These residues correspond to the previously mentioned hydrogenated silicon clusters called fines, which were stuck on the reactor walls in the upper part of the reactor. Their amount clearly increases with the inlet molar fraction of silane, as claimed by Filtvedt et al. [28]. They are in greater quantity here than in other works performed with conventional easy-to-fluidize powders. This is probably due to the tungsten powder’s rather poor ability to fluidize, leading to a lower gas solid contact and then to a higher proportion of homogeneous reactions in the gas bubbles in the bed. Therefore, under the conditions tested, only the lowest inlet

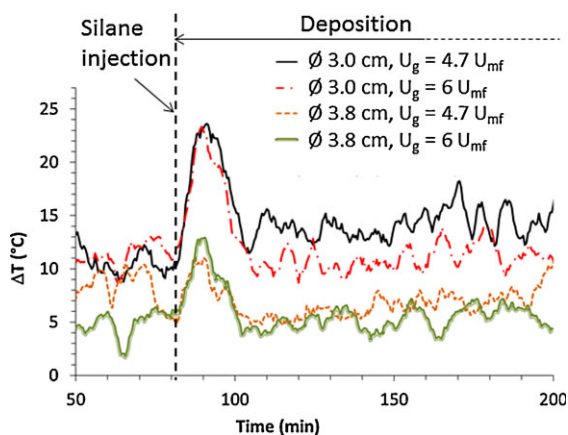


Figure 4 Changes in the bed thermal gradient for various reactor diameters and fluidization ratios ($y_{\text{silane}} = 0.5\%$, 645 °C).

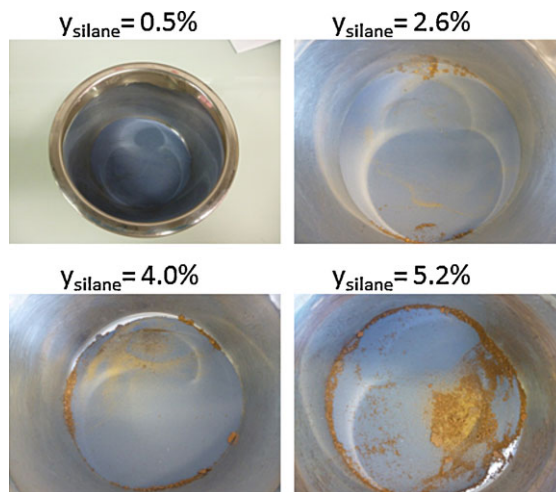


Figure 5 State of the powder after runs 1–4.

molar fraction of silane (0.5%) avoids polluting the coated powder by fines.

3.4 Morphology and composition of the Si deposit SEM examinations and EDX analyses performed on samples prepared with the two previous methods show that the tungsten powder was uniformly coated by a continuous silicon layer as shown in Fig. 6.

Figure 7 shows the morphology of the tungsten surface before and after coating. Before coating, the surface of these particles most likely present a native tungsten oxide layer, and various impurities that form small bumps of several hundred nanometers. For experiments performed with inlet molar fractions of silane higher than 0.5%, the deposit was

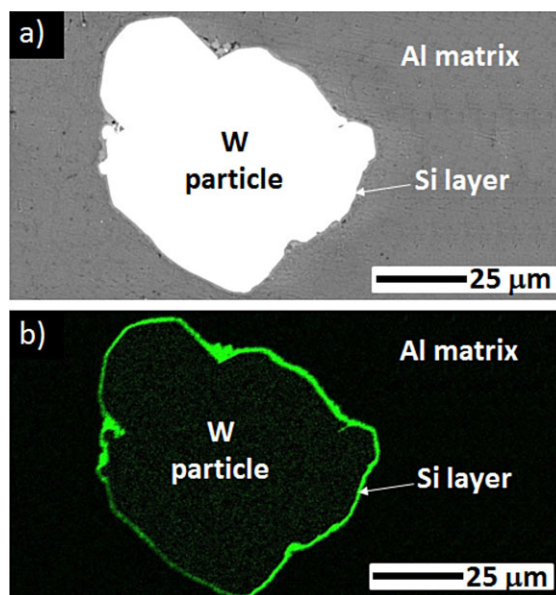


Figure 6 Highlighting of the Si coating on the tungsten particle by EDX analysis (run 4). (a) Electronic image (in electron back scattered mode), (b) Si X-ray map.

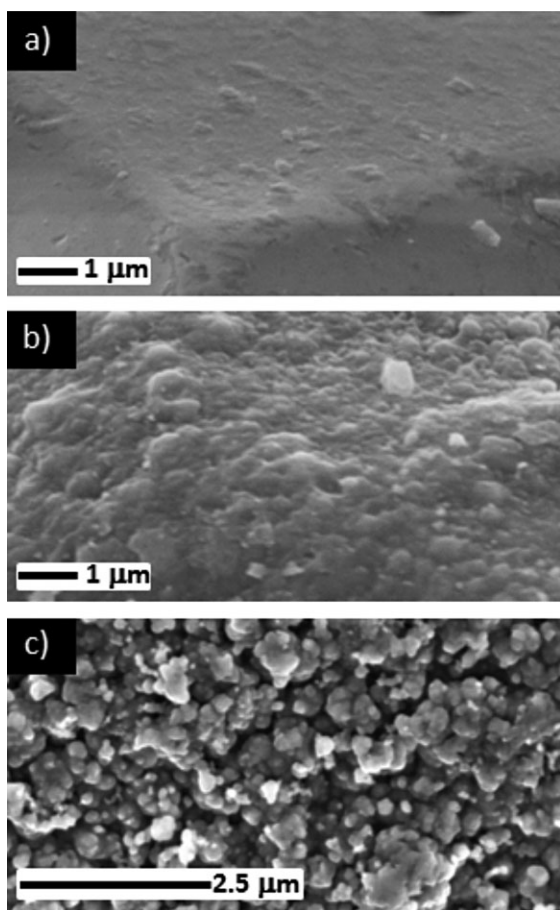


Figure 7 SEM micrographs of the tungsten particles before (a) and after coating with a silane molar fraction of 0.5% (b) and 5.2% (c) (runs 1 and 4).

non-porous, with a grainy aspect, formed of Si nodules, which could indicate that fines contributed to the deposit by scavenging phenomena. The deposit appears smoother for the run performed with 0.5% of silane. Under the conditions tested, it is then likely that this low molar fraction leads to a higher rate of silicon deposition from heterogeneous reactions directly on the powder surface and a much lower amount of fines and scavenging on the tungsten particles. This result is consistent with that of the previous section. Moreover, it is likely that coating adhesion and barrier properties would be better for the lowest silane molar fraction, but these aspects remain to be checked.

Figure 8 shows XRD results, obtained with a 2° grazing incidence, that reveal peaks of tungsten at: 40.3° corresponding to the (110) planes, 58.2° corresponding to the (200) planes, and 73.2° corresponding to the (211) planes. The diffractometer also confirms the presence of silicon which is mainly crystallized, as evidenced by the (111) (at 28.4°) and (220) (at 47.3°) planes. Gao et al. [35] and Schicho et al. [36] found a last peak at 56.1° corresponding to the (311) planes, which is only slightly visible in our case. The spread peak at the beginning of

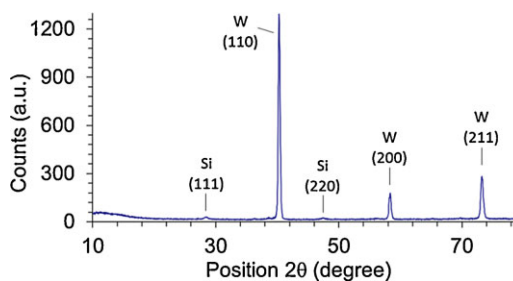


Figure 8 XRD diffractometer of a Si coating performed at 645°C with a molar fraction of silane of 5.2% (run 4).

the diffractometer could correspond to the plastic holder of the powder. In some studies [37, 38], a large peak appears at 23° in the case of the presence of an amorphous phase of silicon oxidized which is difficult to identify in our case. Although the debate is still open, knowing that, some studies on nuclear fuels show that a crystalline coating would retain fission gases better than an amorphous one [39], the crystallized state of our coatings could be a positive feature.

Figure 9a was taken under TEM high resolution conditions in the silicon layer. It reveals crystallographic planes arranged in domains (nano-grains) of several tenths of nm, confirming the previous XRD results on the crystallinity of the deposit.

Figure 9b was taken in STEM mode. It reveals thin dark veins perpendicular to the W/Si interface which can be found in at least half the thickness of the layer. EDX

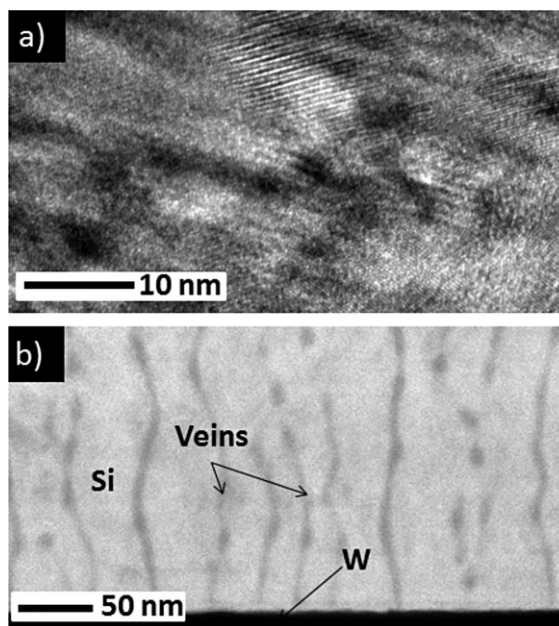


Figure 9 TEM micrographs of a Si coating performed at 645°C with a 2.6% molar fraction of silane (run 2). (a) TEM high resolution image and (b) STEM bright field image.

analyses show that these veins correspond to areas with high tungsten concentrations. These results tend to indicate that tungsten diffuses through the silicon layer during the coating process.

EDX profiles performed at the W/Si interface on the thin sections prepared by the FIB method, show the presence of an oxygen-rich layer with a thickness of the order of 20 nm. That could confirm the presence of a native oxide film. However, it is not possible to assert that it is a tungsten oxide, a silicon one or a mix of oxides.

There is no visible intermediate layer of silicide at the W/Si interface in the samples. Silicides are mentioned by Yoon et al. [40] and Lee et al. [41] with respect to W/Si interactions, with WSi_2 and W_5Si_3 formation at the W/Si interface. However, these studies were performed at higher temperatures of around 1300 °C.

Some impurities comprising Al, O, Fe, Cr, and Ca, and a few porosities were found at the W/Si interface from place to place. The presence of these elements could be explained by impurities already present in the tungsten powders and on the reactor walls.

3.5 Thickness of the deposit and deposition rate The thickness of the silicon layer was determined from SEM examinations (Fig. 10) either on crushed or polished powders, prepared by the two above-mentioned methods.

The coating thickness varied between 120 nm and 1 μ m under the conditions tested, which corresponds to the target thickness range. It increased with the inlet molar fraction of silane.

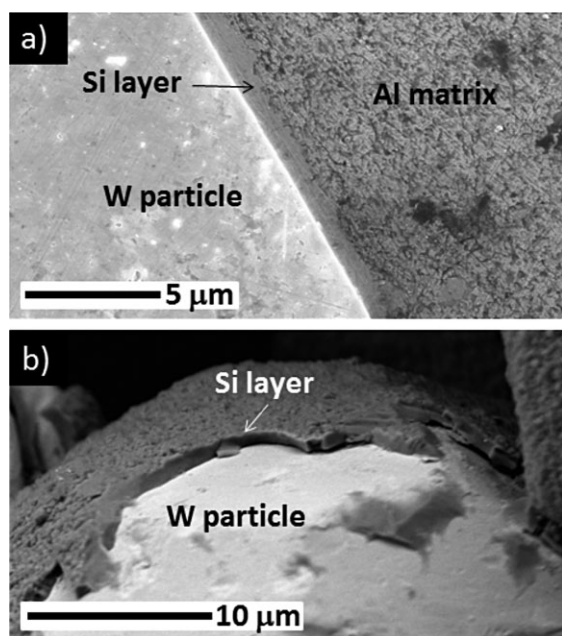


Figure 10 SEM micrographs of the Si coating on a polished particle (a) and on a crushed particle (b) (run 2).

Figure 11 shows the variation in R_d which is the deposition rate in nm/min was estimated from the thicknesses determined by SEM. For each experiment, an average of ten thickness measurements performed by SEM was considered. The deposit has a grainy aspect and bumps and hollows of this coating explain the magnitude of the error bars.

R_d increases almost linearly with the inlet molar fraction of silane, for runs 1–4. This corresponds to deposition rates between 1 and 16 nm/min. Increasing the inlet molar fraction of silane therefore makes it possible to increase the process productivity in terms of the deposition rate, but it decreases the silane conversion rate in the bed by forming higher amounts of fines which pollute the powder. It also creates more intense thermal and pressure drop disturbances involving a higher risk of bed agglomeration.

4 Conclusion Silicon coating of very dense tungsten powder by FB-CVD has been studied at 645 °C for reactors with diameters of 3.0 and 3.8 cm and for inlet molar fractions of silane diluted in argon between 0.5 and 5.2%. The results show that an increase in the inlet molar fraction of silane introduces the risk of partial or total agglomeration of particles in the bed. Upon injection of silane in the reactor, this leads to a temperature gradient between the bottom and the top of the fluidized bed and an increase in the bed pressure drop. This behavior is due to the reactivity of silane, which causes the partial de-fluidization of the bed which is clearly exacerbated by the high density of the tungsten powder.

Post-experimental characterization of the powder revealed that all the tungsten particles were uniformly coated with a continuous silicon layer which was mainly crystallized. The silicon nodules, which made the coating look grainy, increased with the inlet molar fraction of silane. This result associated with the higher amount of hydrogenated silicon fines polluting the bed could indicate that the proportion of homogeneous reactions increase with the inlet molar fraction of silane.

Under the conditions studied, the deposition rate tends to increase with the inlet molar fraction of silane, while the coating thickness tends to range between 120 nm and 1 μ m, which both meet the specifications for U(Mo) coating. The reduction in the reactor diameter from 3.8 to 3.0 cm and a

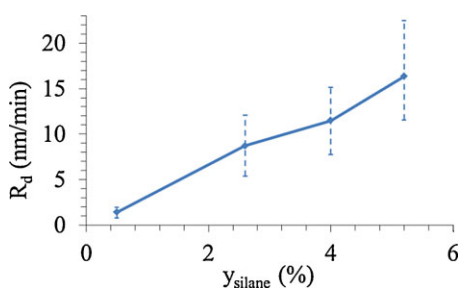


Figure 11 Deposition rate versus the inlet molar fraction of silane (\varnothing 3.8 cm, $U_g/U_{mf} = 4.7$, 645 °C).

modified fluidizing gas velocity, have little impact on the behavior of the process.

These promising results show that the FB-CVD process is able to uniformly coat very dense particles with silicon. Coating experiments on U(Mo) particles are now in progress.

Acknowledgements The authors would like to thank Michel Molinier and Etienne Prevot from the LGC and Nicolas Tarisien and Helene Rouquette from the LCU for their technical support.

References

- [1] S. L. Hayes, M. K. Meyer, G. L. Hofman, and R. V. Strain, Proc. Reduced Enrichment for Research and Test Reactors (RERTR), Sao Paulo, Brazil, 1998.
- [2] M. K. Meyer, G.L. Hofman, J. L. Snelgrove, C. R. Clark, S. L. Hayes, R. V. Strain, J.-M. Park, and K.-H. Kim, Proc. Reduced Enrichment for Research and Test Reactors (RERTR), Budapest, Hungary, 1999.
- [3] S. Dubois, J. Noirrot, J. M. Gatt, and M. Ripert, Proc. Research Reactor Fuel Management (RRFM), Lyon, France, 2007.
- [4] J. M. Hamy, P. Lemoine, F. Huet, C. Jarousse, and J.-L. Emin, Proc. Research Reactor Fuel Management (RRFM), Budapest, Hungary, 2005.
- [5] J. M. Park, H. J. Ryu, Y. S. Lee, B. O. Yoo, Y. H. Jung, and C. K. Kim, Proc. Research Reactor Fuel Management (RRFM), Hamburg, Germany, 2008.
- [6] X. Iltis, F. Charollais, M. Anselmet, P. Lemoine, A. Leenaers, S. Van den Berghe, E. Koonen, C. Jarousse, D. Geslin, F. Frery, and H. Guyon, Proc. Reduced Enrichment for Research and Test Reactors (RERTR), Lisbon, Portugal, 2010.
- [7] S. Van Den Berghe, Y. Parthoens, G. Cornelis, A. Leenaers, E. Koonen, V. Kuzminov, and C. Detavernier, J. Nucl. Mater. **430**, 246–258 (2012).
- [8] S. Van Den Berghe, A. Leenaers, and C. Detavernier, Proc. Research Reactor Fuel Management (RRFM), Marrakesch, Morocco, 2010.
- [9] S. Van Den Berghe, A. Leenaers, and C. Detavernier, Proc. Research Reactor Fuel Management (RRFM), Rome, Italy, 2011.
- [10] A. Leenaers., S. Van den Berghe, E. Koonen, V. Kuzminov, and C. Detavernier, J. Nucl. Mater. **458**, 380–393 (2015).
- [11] J. Chao, J. Lu, H. Yang, M. Zhang, and Q. Liu, Int. J. Heat Mass Tran. **80**, 115–125 (2015).
- [12] C. Vahlas, B. Caussat, P. Serp, and G. N. Angelopoulos, Mater. Sci. Eng. R **53**, 1–72 (2006).
- [13] S. Bong-Kuk, A. Kazuki, K. Katsuki, and M. Shigeharu, J. Membrane Sci. **146**, 73–82 (1998).
- [14] D. C. Lim, H. G. Jee, J. W. Kim, J. S. Moon, S. B. Lee, S. S. Choi, and J. H. Boo, Thin Solid Films **459**, 7–12 (2004).
- [15] E. De Paola and P. Duvemeuil, Comput. Chem. Eng. **22**, 683–686 (1998).
- [16] A. Petit and M. Zeman, in: SAFE 2001: Proceedings CD-ROM, pp. 150–153 (2001).
- [17] T. E. Wilke, K. A. Turner, and C. J. Takoudis, Chem. Eng. Sci. **41**, 643–650 (1986).
- [18] I. Brunets, A. A. I. Aarnink, A. Boogaard, A. Y. Kovalgin, R. A. M. Wolters, J. Holleman, and J. Schmitz, Surf. Coat. Technol. **201**, 9209–9214 (2007).
- [19] A. A. Onischuk, A. I. Levykin, V. P. Strunin, K. K. Sabelfeldt, and V. N. Panlov, J. Aerosol Sci. **31**, 1263–1281 (2000).
- [20] M. T. Swihart and S. L. Girshick, J. Phys. Chem. B **103**, 64–76 (1999).
- [21] S. S. Talukdar and M. T. Swihart, J. Aerosol Sci. **35**, 889–908 (2004).
- [22] L. Zambov, J. Cryst. Growth **125**, 164–174 (1992).
- [23] T. R. Hogness, T. L. Wilson, and W. C. Johnson, J. Am. Chem. Soc. **58**, 108–112 (1936).
- [24] M. E. Coltrin, R. J. Kee, and J. A. Miller, J. Electrochem. Soc. **11**, 425–434 (1984).
- [25] W. G. Breiland, M. E. Coltrin, and P. Ho, J. Appl. Phys. **59**, 3267–3273 (1986).
- [26] M. A. Ring, M. J. Punentes, and H. E. O’Neal, J. Am. Chem. Soc. **92**, 4845–4848 (1970).
- [27] L. Cadoret, N. Reuge, S. Pannala, M. Syamlal, C. Rossignol, J. Dexpert-Ghys, C. Coufort, and B. Caussat, Powder Technol. **190**, 185–191 (2009).
- [28] W. O. Filtvedt, A. Holt, P. A. Ramachandran, and M. C. Melaen, Sol. Energy Mater. Sol. Cells **107**, 188–200 (2012).
- [29] D. Geldart, Gas Fluidization Technology (John Wiley & Sons, New York, 1986).
- [30] Ph. Rodriguez, B. Caussat, C. Ablitzer, X. Iltis, and M. Brothier, Chem. Eng. Res. Des. **91**, 2477–2483 (2013).
- [31] T. Kojima, H. Hiroha, K. Iwata, and T. Furusawa, Int. Chem. Eng. **32**, 739–749 (1992).
- [32] B. Caussat, M. Hémati, and J. P. Couderc, Chem. Eng. Sci. **50**, 3615–3624 (1995).
- [33] J. R. R. Ruvalcaba, B. Caussat, and M. H. Couderc, Chem. Eng. J. **73**, 61–66 (1999).
- [34] M. P. Tejero-Ezpelata, S. Buchholz, and L. Mleczko, Can. J. Chem. Eng. **82**, 520–529 (2004).
- [35] J. Gao, L. Zhang, J. Xiao, J. Gong, C. Sun, and L. Wen, Mater. Lett. **68**, 367–369 (2012).
- [36] S. Schicho, F. Kohler, R. Carius, and A. Gordijn, Sol. Energy Mater. Sol. Cells **98**, 391–397 (2012).
- [37] Y. Li, L. Wang, S. Yin, and F. Yang, Mater. Chem. Phys. **141**, 874–881 (2013).
- [38] L. Qi, Z. Hu, W. Li, X. Qin, G. Du, W. Han, and W. Shi, Mater. Sci. Semicond. Proc. **15**, 412–420 (2012).
- [39] S. Van den Berghe, A. Leenaers, E. Koonen, and L. Sannen, Adv. Sci. Technol. **73**, 78–90 (2010).
- [40] J.-K. Yoon, K.-W. Lee, S.-J. Chung, I.-J. Shon, J.M. Doh, and G.-H. Kim, J. Alloy. Compd. **420**, 199–206 (2006).
- [41] K.-W. Lee, J.-K. Yoon, J.-K. Lee, J.-M. Doh, K.-T. Hong, and W.-Y. Yoon, Surf. Coat. Technol. **187**, 146–153 (2004).